High-Precision Q-Value Measurement Confirms the Potential of ^{135}Cs for Absolute Antineutrino Mass Scale Determination

A. de Roubin, * J. Kostensalo, T. Eronen, L. Canete, † R. P. de Groote, A. Jokinen, A. Kankainen, D. A. Nesterenko, I. D. Moore, S. Rinta-Antila, J. Suhonen, and M. Vilén ‡
University of Jyväskylä, P.O. Box 35, FI-40014 Jyväskylä, Finland

(Received 20 February 2020; revised manuscript received 10 April 2020; accepted 7 May 2020; published 5 June 2020)

The ground-state-to-ground-state β-decay Q value of ^{135}Cs$(7/2^+) \rightarrow {}^{135}Ba(3/2^+)$ has been directly measured for the first time. The measurement was done utilizing both the phase-imaging ion-cyclotron resonance technique and the time-of-flight ion-cyclotron resonance technique at the JYFLTRAP Penning-trap setup and yielded a mass difference of 268.66(30) keV between ^{135}Cs$(7/2^+)$ and ^{135}Ba$(3/2^+)$. With this very small uncertainty, this measurement is a factor of 3 more precise than the currently adopted Q value in the Atomic Mass Evaluation 2016. The measurement confirms that the first-forbidden unique β^--decay transition ^{135}Cs$(7/2^+) \rightarrow {}^{135}Ba(11/2^-)$ is a candidate for antineutrino mass measurements with an ultralow Q value of 0.44(31) keV. This Q value is almost an order of magnitude smaller than those of nuclides presently used in running or planned direct (anti)neutrino mass experiment.

DOI: 10.1103/PhysRevLett.124.222503

The determination of the absolute scale of neutrino masses is one of the most important and intriguing goals in particle physics. In laboratory-based experiments this can be addressed by observation of neutrinoless double β decay whose half-life can be related to the effective Majorana mass [1] or by the analysis of the end point region of β decay and electron capture experiments which is sensitive to an effective electron (anti)neutrino mass [2]. The β decay and electron capture experiments are model-independent methods to directly infer the effect of massive neutrinos by kinematical analysis, as in the KATRIN [2] and MARE [3] experiments using ^{3}H and ^{187}Re, respectively, or from the electron capture decay, as in the ECHo [4] and in the HOLMES [5] experiments using ^{163}Ho. In these experiments one strives for sub-electron-volt mass sensitivity, which necessitates the use of nuclear decays of as small as possible decay energy (Q value) in order to maximize the fraction of events in the region of interest, i.e., close to the end point. The corresponding Q values are $Q_\beta = 18.5718(12)$ keV for the tritium decay [6], $Q_\beta = 2.4666(16)$ keV for ^{187}Re decay [7], and $Q_{\mathrm{EC}} = 2.858(10)(50)$ keV for ^{163}Ho electron capture decay [8] with statistical and systematic uncertainties, respectively.

The β decay of the $7/2^+$ state of ^{135}Cs to the $11/2^-$ state of ^{135}Ba has been proposed as a candidate for effective electron antineutrino mass measurements, see [9]. However, it has not been clear if it is energetically allowed. The decay has never been observed directly and the low Q value has been deduced from the well known excitation energy of the $11/2^-$ state at 268.218(20) keV in ^{135}Ba [10,11] (see Fig. 1) and the ground-state-to-ground-state (GS-to-GS) β-decay Q value. Based on the AME2016 [11] the GS-to-GS Q value is equal to 268.9(10) keV. In AME2016, the mass of ^{135}Cs is tied to the very precisely known ^{133}Cs mass through (n, γ) measurements and determines the mass of ^{135}Cs with a weight of nearly 100%. The mass of ^{135}Ba is derived from (n, γ) links between ^{134}Ba–^{135}Ba and ^{135}Ba–^{136}Ba, which contribute to the ^{135}Ba mass by 54.9% and 45.1%, respectively. Through Penning trap Q-value measurements, the ^{136}Ba mass links to the mass of the ^{136}Xe, which is known very precisely. ^{134}Ba links to ^{133}Cs through the β decay of ^{134}Cs and (n, γ). From this, the decay to the $11/2^-$ state has a Q value of 0.5

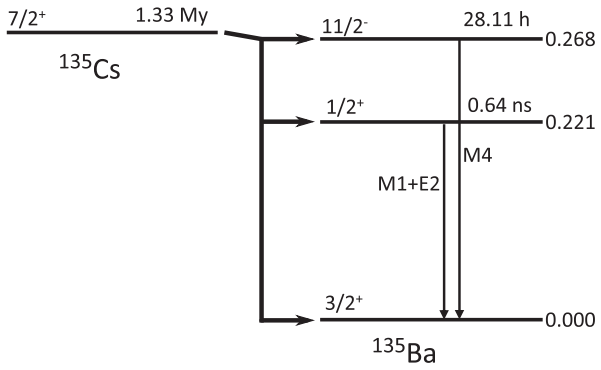

FIG. 1. β^- decay of the ground state of ^{135}Cs to the ground state and first two excited states in ^{135}Ba. The as yet undetected transition to the second excited state $(11/2^-)$ is an ultralow Q-value transition relevant for the effective antineutrino mass measurements. The transition to the first excited state $(1/2^+)$ is greatly hindered by the large change in angular momentum. The numbers to the right of the energy levels are excitation energies in megaelectron-volt.

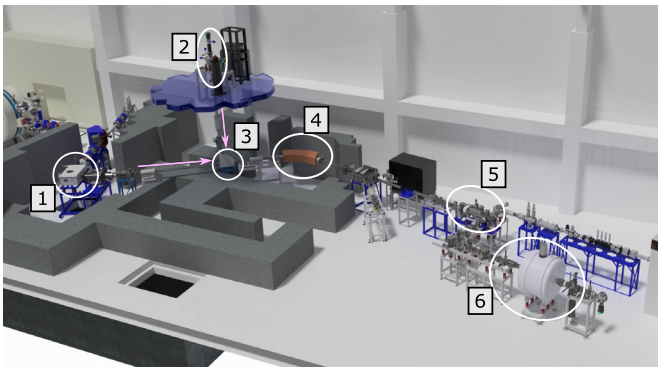

FIG. 2. Layout of the IGISOL facility. The radioactive $^{135}Cs^{+}$ ions were produced with proton-induced fission reactions (1), the stable $^{135}Ba^{+}$ ions with an off-line source (2). The beam from either source was selected with an electrostatic kicker (3). The mass number selection was performed with a dipole magnet (4), the ion bunching with the cooler buncher (5), and finally the mass-difference measurement with the JYFLTRAP Penning trap setup (6) [18].

(12) keV. Although the value is more precise, it does not reliably exclude whether the decay to the $11/2^{-}$ state is energetically possible or not. In this Letter, we report on the first direct Q-value measurement of the β decay of ^{135}Cs in order to verify whether the transition $^{135}\mathrm{Cs}(7/2^{+}) \rightarrow {}^{135}\mathrm{Ba}(11/2^{-})$ could serve as a potential candidate for very low Q-value effective electron antineutrino mass measurements.

The GS-to-GS Q value of ^{135}Cs was measured using the JYFLTRAP double Penning trap setup mass spectrometer at the Ion Guide Isotope Separator On-Line (IGISOL) facility [12,13], see Fig. 2. The $^{135}\mathrm{Cs}(7/2^{+})$ ions were produced using proton-induced fission with a 50-MeV proton beam impinging into a $^{\mathrm{nat}}$U target. For high-precision Penning trap mass measurements it is of utmost importance to have a monoisotopic sample of ions. Since it is not possible to separate $^{135}\mathrm{Ba}(11/2^{-})$ and $^{135}\mathrm{Cs}(7/2^{+})$ that have nearly identical mass with currently available separation techniques [14,15], a fission reaction was chosen to produce ^{135}Cs ions. Based on a semiempirical fit to the independent fission yield data to theoretical models [16], the $^{135}\mathrm{Ba}(11/2^{-})$ yield was expected to be a factor of 100 less than $^{135}\mathrm{Cs}(7/2^{+})$. The reference $^{135}\mathrm{Ba}(3/2^{+})$ ions were separately produced with an off-line glow-discharge ion source [17].

The ion beams, irrespective of the source, were coarsely mass separated to contain only $A/q = 135$ ions with a dipole magnet, where A is the mass number and q is the charge state of the ion (the typical ionization state is $+1$), and injected into the radio-frequency cooler-buncher. The resulting bunched beams were delivered to the purification Penning trap, where the ions were selected using the buffer gas cooling cleaning technique [19]. An additional Ramsey cleaning [14] step in the precision trap was needed to remove $^{135}Xe^{+}$, $^{135m}Xe^{+}$, and $^{135}I^{+}$. After the purification process a contamination level on the order of 1% of the data was observed in the measurement trap. However, the contaminant ions were well separated from the ions of interest by the phase-imaging ion-cyclotron resonance (PI-ICR) technique [15,20] and gated away for the analysis. A detailed ion rate dependency analysis [21] to probe for frequency shifts as a function of ion number did not show any significant deviations in the results.

Both the time-of-flight ion-cyclotron resonance (TOF-ICR) [22,23] technique utilizing Ramsey's method of time-separated oscillatory fields [24,25] and the newly commissioned PI-ICR [15,20] method were used for the mass-difference (Q-value) measurement. Both of the techniques provide the free-space cyclotron frequency

$$\nu_c = \frac{1}{2\pi}\frac{q}{m}B, \tag{1}$$

where q/m is the charge-to-mass ratio of the ion and B the magnetic field. The Q-value formula is

$$Q = m_p - m_d = (R-1)(m_d - m_e), \tag{2}$$

where m_p and m_d are the masses of the parent $[^{135}\mathrm{Cs}(7/2^{+})]$ and daughter $[^{135}\mathrm{Ba}(3/2^{+})]$ atom, $R = \nu_d/\nu_p$ is their cyclotron frequency ratio for singly charged ions, and m_e is the electron rest mass. Since $(R-1) < 10^{-5}$, the 0.3 keV/c^2 uncertainty in the mass of $^{135}\mathrm{Ba}(3/2^{+})$ [11] is not a limitation for a high-precision measurement. As the measured doublet has the same mass value A, mass-dependent errors become negligible [26]. Contribution from the atomic electron binding energies is on the order of electron-volt and thus can be neglected here.

The Ramsey-type TOF-ICR cyclotron frequency measurements were performed for approximately 10 h with a 25-350–25 ms (on-off-on) excitation pattern. The measurement was alternated between parent and daughter ions every five scan rounds (about 2 min). A TOF-ICR resonance curve obtained using the Ramsey method, collected for 1.5 h, is shown in Fig. 3.

Data with the PI-ICR technique were collected for about 18 h. The two phase spots, "magnetron" and "cyclotron," left and right panel in Fig. 4, respectively, were collected using the timing patterns as described in [15]. The two phase spots were collected consecutively to account for any temporal shifts in the ion positions. The center spot is obtained by storing the ions in the trap for a few milliseconds and then extracting them. The extraction delay was varied over one magnetron period to account for any residual magnetron motion that could shift the different spots. The center spots were collected in approximately three-hour intervals. The parent and daughter ion measurements were switched every few minutes.

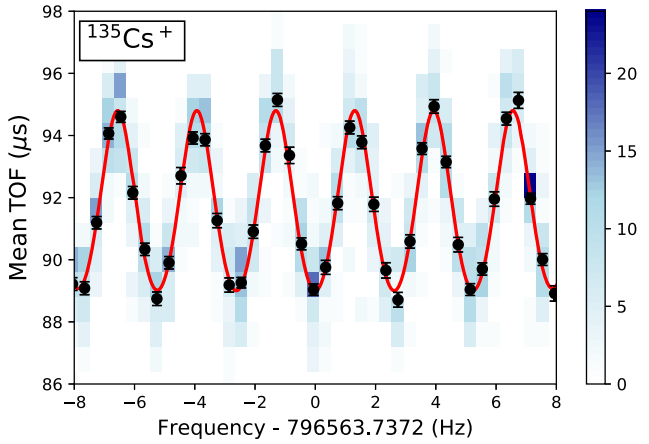

FIG. 3. Ramsey TOF-ICR spectrum for $^{135}Cs^{+}$ ions using 25-350–25 ms (on-off-on) excitation pattern. The mean data points are shown in black, the fit of the theoretical curve [27] in red. The blue-shaded squares indicate the number of ions in each time-of-flight bin.

The TOF-ICR and PI-ICR data were split to 3 and 7 parts, respectively, for final fitting. Both types of measurements were checked for any count-rate related frequency shifts [21]. Since no such shifts were observed, all bunches with up to 5 ions were used in the analysis. Temporal fluctuations of the B field contribute less than 10^{-10} to the final frequency ratio uncertainty since the parent-daughter measurements were interleaved every few minutes [28]. Likewise, frequency shifts in the PI-ICR measurement due to ion image distortions are well below the statistical uncertainty and thus were not added to the final uncertainty.

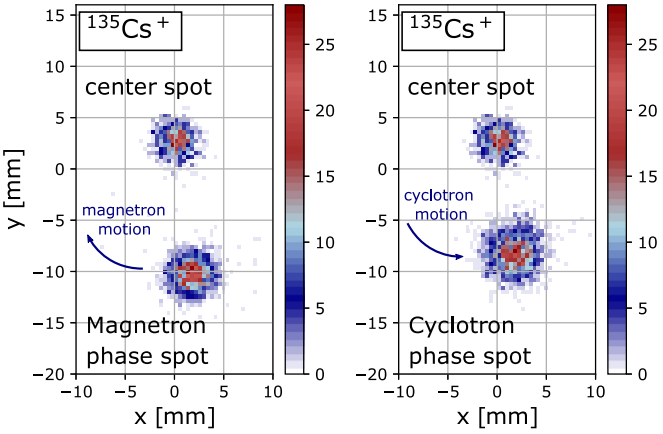

FIG. 4. The three different ion spots (center, magnetron phase, and cyclotron phase) of $^{135}Cs^{+}$ on the 2D position-sensitive microchannel plate detector after a typical PI-ICR excitation pattern. On the left, the magnetron phase spot is shown, on the right the cyclotron phase spot. The angle difference between the two spots is related to the cyclotron frequency of the ion species. The number of ions in each pixel is indicated by color bars (colors in the online version).

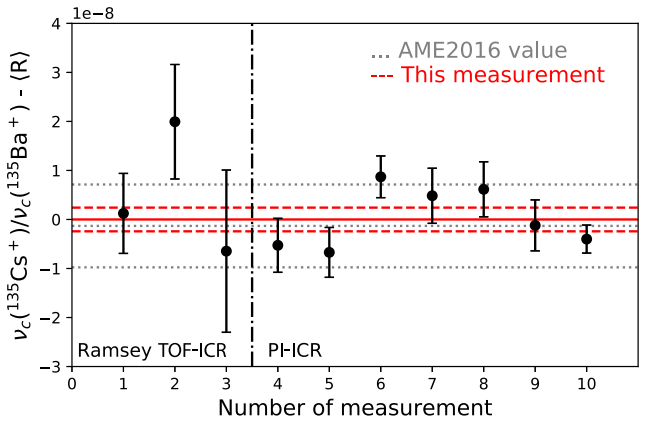

FIG. 5. Difference between the cyclotron frequency ratios $\nu_c(^{135}Cs^{+})/\nu_c(^{135}Ba^{+})$ measured in this work, shown as black data points, and the weighted average value from this work $\langle R\rangle = 1.000\,002\,138\,0(24)$ represented by the solid red line and its uncertainty in red dashed lines. The dotted gray lines represent the difference between our new value and the one referred to in the AME2016 [11] with its uncertainty.

The results of the analysis, including all data from both Ramsey-type TOF-ICR and PI-ICR measurements with comparison to literature values, are plotted in Fig. 5. The final results for the mean cyclotron frequency ratio between the daughter and parent nuclei and the corresponding Q value are compared to literature values in Table I.

The new Q value is a factor of 3 more precise than that derived from masses of ^{135}Cs and ^{135}Ba given in AME2016 ([11] and references therein) and is equal to 268.66 (30) keV. It confirms that both the second-forbidden unique transition to the first excited state $(1/2^{+})$ and the first-forbidden unique transition to the second excited state $(11/2^{-})$ in ^{135}Ba can occur with Q values of 47.69(31) and 0.44(31) keV, respectively. Decay to the $3/2^{+}$ ground state of ^{135}Ba has a half-life $(1.3-1.6)\times 10^{6}$ yr [30]. With the presently computed half-life estimate $(1-300)\times 10^{11}$ yr (see below) for the transition to the $11/2^{-}$ state, the branching to this state is about $(0.04\text{–}16)\times 10^{-6}$. This branching ratio is close to that measured for the ultralow-Q-value β^{-} transition $^{115}In(9/2^{+}) \rightarrow {}^{115}Sn(3/2^{+})$ in [31], 1.1×10^{-6}. Hence, it is feasible to detect the $^{135}Cs(7/2^{+}) \rightarrow {}^{135}Ba(11/2^{-})$ transition. This and the fact

TABLE I. Final result from the analysis with $\langle R\rangle$ being the mean cyclotron frequency ratio between the daughter and parent nuclei. The corresponding Q value is also given as well as its comparison to the Q value referred in the AME2016 [11].

$\langle R\rangle = \nu_{c,d}/\nu_{c,p}$	1.000 002 138 0(24)
Q_{β^-} (this work)	268.66(30) keV
Q_{β^-} (AME2016 [11])	268.9(10) keV
Q_{β^-} ([29])	210(10) keV

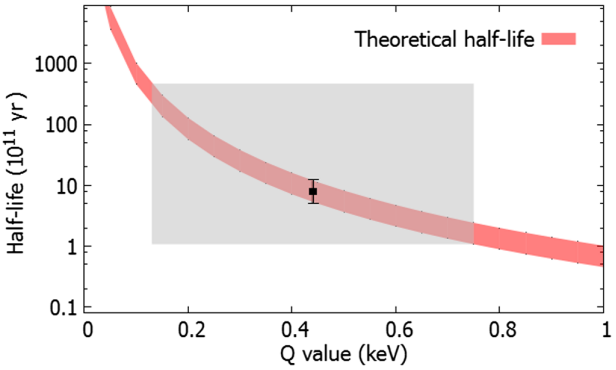

FIG. 6. Shell-model calculated partial half-life of the decay of ^{135}Cs to the second excited state in ^{135}Ba as a function of the Q value newly obtained: The red band corresponds to the range $g_A^{\text{eff}} = 0.8$–1.2 of values of the axial coupling. The gray horizontal stripe gives the half-life assuming the best estimate $Q = 0.44(31)$ keV from the present work.

that the transition has a simple unique (universal) shape of the electron spectrum and an ultralow Q value of only 0.44(31) keV make this transition an excellent candidate for neutrino mass measurements.

In order to estimate the partial half-lives for the transitions to the excited states, we have run large-scale shell-model calculations using the computer code NuShellX@MSU [32]. The calculations were done in a model space consisting of the orbitals $0g_{7/2}$, $1d$, $2s$, and $0h_{11/2}$ for both protons and neutrons with the effective Hamiltonian Sn100pn [33]. The shell-model calculations performed here represent a significant improvement over those performed in [9], where the microscopic quasiparticle-phonon model (MQPM) [34,35] was used to compute the involved nuclear wave functions. Since the present shell-model calculations are much more sophisticated than the old MQPM calculations the computational time required is several thousand times that needed in [9]. The uncertainties related to the theoretical half-lives stem mostly from the unknown effective value g_A^{eff} of the axial-vector coupling. In Fig. 6 we plot the partial half-life of the transition to the $11/2^-$ state as a function of the Q value. The red band corresponds to the conservative interval $g_A^{\text{eff}} = 0.8$–1.2 deduced from a large body of related investigations [36]. Since the decays to the excited state are forbidden unique, the half-lives are simply proportional to g_A^{-2}, and one can easily derive half-life estimates for any choice of g_A^{eff}.

The calculated partial half-lives of the excited-state transitions are given in Table II. Here, the uncertainties arise from the assumed interval $g_A^{\text{eff}} = 0.8$–1.2 for the axial coupling. Also, the MQPM-computed half-lives, deduced from [9], are given for comparison. As can be seen, the presently computed partial half-lives deviate substantially from those deduced from [9]. It should be noted that the ratio of the two half-lives, about 100 for the present calculation and about 5 orders of magnitude for the calculation of Mustonen *et al.* [9], depends on two competing features. The one unit of difference in the forbiddenness makes the decay to the $11/2^-$ state some 4 orders of magnitude faster than the decay to the $1/2^+$ state [37]. On the other hand, the roughly 100 times larger Q value of the $1/2^+$ transition makes this transition faster by a couple orders of magnitude [38], the net effect being that the transition to the $11/2^-$ state can be estimated to be approximately 2 orders of magnitude faster than the transition to the $1/2^+$ state, in agreement with the results of the present shell-model calculation.

TABLE II. The Q values and half-lives for the transitions of ^{135}Cs$(7/2^+)$ to the two excited states in ^{135}Ba. The half-life uncertainty for the transition to the $11/2^-$ state includes only the one stemming from the nuclear-structure model (interacting shell model, ISM). The uncertainty related to the Q value is one order of magnitude for this transition, while it is negligible for the transition to the $1/2^+$ state.

Transition to	^{135}Ba$(1/2^+)$	^{135}Ba$(11/2^-)$
Q value (keV)	47.69(31)	0.44(31)
$T_{1/2}$ (ISM) (y)	$6.5(17) \times 10^{13}$	$8.2(32) \times 10^{11}$
$T_{1/2}$ (MQPM) (y) [9]	2×10^{15}	3×10^{10}

A nuclear decay of as small energy as possible favors a larger fraction of the number of events in the region close to the end point and can prove particularly useful in the investigation of the effective electron antineutrino mass. In this framework, the β-decay Q value of the transition from the $7/2^+$ ground state of ^{135}Cs to the $3/2^+$ ground state of ^{135}Ba was measured with high precision at the JYFLTRAP Penning trap setup. This is the first direct determination of the Q value. The new precise measurement confirms that the Q value of the β^--decay transition $^{135}\text{Cs}(7/2^+) \rightarrow {}^{135}\text{Ba}(11/2^-)$ is positive with an ultralow Q value of 0.44(31) keV. Hence, this first-forbidden unique transition, with a simple universal spectral shape, has the potential to serve as a candidate for effective electron antineutrino mass measurements with an almost order of magnitude lower Q value than in presently running or planned direct (anti)neutrino mass experiments. However, one should note here that for a realistic measurement of the β spectrum related to the decay to the $11/2^-$ excited state, a coincidence with the deexcitation gamma ray would be extremely important. Unfortunately, in this case it would not be an easy task as the $11/2^-$ excited state has a half-life $T_{1/2} = 28$ h with respect to the emission of the β particle.

This work has been supported by the Academy of Finland under the Finnish Centre of Excellence Programme 2012–2017 (Nuclear and Accelerator Based Physics Research at JYFL) and Projects No. 306980,

No. 312544, No. 275389, No. 284516, and No. 295207. This work was supported by the EU Horizon 2020 research and innovation program under Grant No. 771036 (ERC CoG MAIDEN).

*Present address: Centre d'Etudes Nucléaires de Bordeaux Gradignan, CNRS/IN2P3—Université de Bordeaux, 33175 Gradignan Cedex, France.
deroubin@cenbg.in2p3.fr
†Present address: University of Surrey, Guildford, Surrey, GU2 7XH, U.K.
‡Present address: CERN, 1211 Geneva, Switzerland.

[1] H. Ejiri, J. Suhonen, and K. Zuber, Phys. Rep. **797**, 1 (2019).
[2] M. Aker *et al.* (KATRIN Collaboration), Phys. Rev. Lett. **123**, 221802 (2019).
[3] E. Ferri *et al.* (MARE Collaboration), Phys. Procedia **61**, 227 (2015).
[4] L. Gastaldo *et al.* (ECHo Collaboration), Eur. Phys. J. Special Topics **226**, 1623 (2017).
[5] M. Faverzani *et al.*, J. Low Temp. Phys. **184**, 922 (2016).
[6] E. W. Otten and C. Weinheimer, Rep. Prog. Phys. **71**, 086201 (2008).
[7] D. A. Nesterenko, S. Eliseev, K. Blaum, M. Block, S. Chenmarev, A. Dörr, C. Droese, P. E. Filianin, M. Goncharov, E. Minaya Ramirez, Y. N. Novikov, L. Schweikhard, and V. V. Simon, Phys. Rev. C **90**, 042501(R) (2014).
[8] P. C.-O. Ranitzsch, C. Hassel, M. Wegner, D. Hengstler, S. Kempf, A. Fleischmann, C. Enss, L. Gastaldo, A. Herlert, and K. Johnston, Phys. Rev. Lett. **119**, 122501 (2017).
[9] M. T. Mustonen and J. Suhonen, Phys. Lett. B **703**, 370 (2011).
[10] F. Bazan and R. Meyer, Nucl. Phys. **A164**, 552 (1971).
[11] M. Wang, G. Audi, F. G. Kondev, W. Huang, S. Naimi, and X. Xu, Chin. Phys. C **41**, 030003 (2017).
[12] J. Äystö, Nucl. Phys. **A693**, 477 (2001).
[13] I. D. Moore, T. Eronen, D. Gorelov, J. Hakala, A. Jokinen, A. Kankainen, V. Kolhinen, J. Koponen, H. Penttilä, I. Pohjalainen, M. Reponen, J. Rissanen, A. Saastamoinen, S. Rinta-Antila, V. Sonnenschein, and J. Äystö, Nucl. Instrum. Methods Phys. Res., Sect. B **317**, 208 (2013).
[14] T. Eronen, V.-V. Elomaa, U. Hager, J. Hakala, A. Jokinen, A. Kankainen, S. Rahaman, J. Rissanen, C. Weber, and J. Äystö, Nucl. Instrum. Methods Phys. Res., Sect. B **266**, 4527 (2008).
[15] D. A. Nesterenko, T. Eronen, A. Kankainen, L. Canete, A. Jokinen, I. D. Moore, H. Penttilä, S. Rinta-Antila, A. de Roubin, and M. Vilen, Eur. Phys. J. A **54**, 154 (2018).
[16] H. Penttilä *et al.*, Eur. Phys. J. A **52**, 104 (2016).
[17] M. Vilen, L. Canete, B. Cheal, A. Giatzoglou, R. de Groote, A. de Roubin, T. Eronen, S. Geldhof, A. Jokinen, A. Kankainen, I. Moore, D. Nesterenko, H. Penttilä, I. Pohjalainen, M. Reponen, and S. Rinta-Antila, Nucl. Instrum. Methods Phys. Res., Sect. B **463**, 382 (2020).
[18] T. Eronen, V. Kolhinen, V. V. Elomaa, D. Gorelov, U. Hager, J. Hakala, A. Jokinen, A. Kankainen, P. Karvonen, S. Kopecky, I. D. Moore, H. Penttilä, S. Rahaman, S. Rinta-Antila, J. Rissanen, A. Saastamoinen, J. Szerypo, C. Weber, and J. Äystö, Eur. Phys. J. A **48**, 46 (2012).
[19] G. Savard, S. Becker, G. Bollen, H.-J. Kluge, R. Moore, T. Otto, L. Schweikhard, H. Stolzenberg, and U. Wiess, Phys. Lett. **158A**, 247 (1991).
[20] S. Eliseev, K. Blaum, M. Block, C. Droese, M. Goncharov, E. Minaya Ramirez, D. A. Nesterenko, Y. N. Novikov, and L. Schweikhard, Phys. Rev. Lett. **110**, 082501 (2013).
[21] A. Kellerbauer, K. Blaum, G. Bollen, F. Herfurth, H.-J. Kluge, M. Kuckein, E. Sauvan, C. Scheidenberger, and L. Schweikhard, Eur. Phys. J. D **22**, 53 (2003).
[22] G. Gräff, H. Kalinowsky, and J. Traut, Z. Phys. A **297**, 35 (1980).
[23] M. König, G. Bollen, H.-J. Kluge, T. Otto, and J. Szerypo, Int. J. Mass Spectrom. Ion Process. **142**, 95 (1995).
[24] M. Kretzschmar, AIP Conf. Proc. **457**, 242 (1999).
[25] S. George, S. Baruah, B. Blank, K. Blaum, M. Breitenfeldt, U. Hager, F. Herfurth, A. Herlert, A. Kellerbauer, H.-J. Kluge, M. Kretzschmar, D. Lunney, R. Savreux, S. Schwarz, L. Schweikhard, and C. Yazidjian, Phys. Rev. Lett. **98**, 162501 (2007).
[26] C. Roux, K. Blaum, M. Block, C. Droese, S. Eliseev, M. Goncharov, F. Herfurth, E. M. Ramirez, D. A. Nesterenko, Y. N. Novikov, and L. Schweikhard, Eur. Phys. J. D **67**, 146 (2013).
[27] M. Kretzschmar, Int. J. Mass Spectrom. **264**, 122 (2007).
[28] L. Canete, A. Kankainen, T. Eronen, D. Gorelov, J. Hakala, A. Jokinen, V. S. Kolhinen, J. Koponen, I. D. Moore, J. Reinikainen, and S. Rinta-Antila, Eur. Phys. J. A **52**, 124 (2016).
[29] N. Sugarman, Phys. Rev. **75**, 1473 (1949).
[30] C. M. MacDonald, R. J. Cornett, C. R. J. Charles, X. L. Zhao, and W. E. Kieser, Phys. Rev. C **93**, 014310 (2016).
[31] J. S. E. Wieslander, J. Suhonen, T. Eronen, M. Hult, V.-V. Elomaa, A. Jokinen, G. Marissens, M. Misiaszek, M. T. Mustonen, S. Rahaman, C. Weber, and J. Äystö, Phys. Rev. Lett. **103**, 122501 (2009).
[32] B. A. Brown and W. D. M. Rae, Nucl. Data Sheets **120**, 115 (2014).
[33] B. A. Brown, N. J. Stone, J. R. Stone, I. S. Towner, and M. Hjorth-Jensen, Phys. Rev. C **71**, 044317 (2005).
[34] J. Toivanen and J. Suhonen, J. Phys. G. **21**, 1491 (1995).
[35] J. Toivanen and J. Suhonen, Phys. Rev. C **57**, 1237 (1998).
[36] J. T. Suhonen, Front. Phys. **5**, 55 (2017).
[37] J. Kostensalo and J. Suhonen, Phys. Rev. C **95**, 014322 (2017).
[38] H. Behrens and W. Bühring, *Electron Radial Wave Functions and Nuclear Beta Decay* (Clarendon, Oxford, 1982).